MODERN DESIGN OF A TWO-STAGE BLOWER FOR TANK AERATORS

Andrei DRAGOMIRESCU[1], Adrian CIOCĂNEA[2]

The paper presents a new design of a two-stage blower used for tank aerators, working at high rotation speed, validated by numerical simulations and experiments. The simulations were performed for one stage of the blower operating at the rated speed. Laboratory tests were carried out on a prototype blower operating at 1/3 of the rated speed and additional simulations were performed. The numerical results are found to be in good agreement with the test ones: the blower fulfils the demands in terms of volume flow rate and output pressure specified for designing a series of similar turbomachines. By using the presented numerical algorithms employed for the numerical simulations, the working parameters of the blower can be assessed before the manufacturing process and design improvements can be provided at low costs.

Keywords: two-stage blower, design, validation, CFD, performance curves.

1. Introduction

Tank aerators are commonly used in water treatment plants to improve the quality of waste water. Inside a tank aerator, either coarse or fine air bubbles are released at the bottom through spargers that are usually either plates with orifices or porous diffusers. The bubbles rise to the surface under the combined effect of buoyant and drag forces, inducing a mixing of the waste water inside the tank and transferring oxygen to that water at a lower or higher rate, depending on bubble size. The minimum pressure of the supplied air must equal the pressure drop across the sparger plus the hydrostatic pressure corresponding to the highest possible water level inside the tank aerator. Since the water level can be as high as 3 to 5 m and the pressure drop across the spargers is not negligible, blowers or low pressure compressors are required to pump the air.

In this paper, the design of a two-stage blower for tank aerators is firstly verified by means of numerical simulations in order to assess, before manufacturing the blower, the degree to which the machine is able to deliver the volume flow rate and total pressure considered for the design point. Secondly, the

[1] Assist. Prof., Faculty of Power Engineering, University POLITEHNICA of Bucharest, Romania, andrei.dragomirescu@upb.ro
[2] Prof., Faculty of Power Engineering, University POLITEHNICA of Bucharest, Romania, adrian.ciocanea@upb.ro

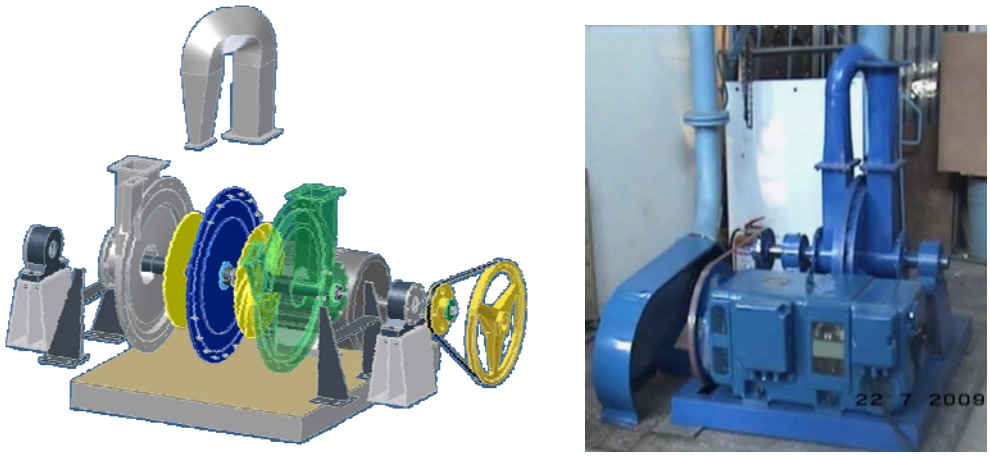

Fig. 1. The two-stage blower

paper also presents experimental results obtained after manufacturing the blower and testing it according to corresponding norms.

The two-stage blower has two impellers mounted back to back on the same shaft supported by two roller bearings (Fig. 1). Pumped air is delivered from one stage to the other through a short connection pipe of rectangular cross-section. An electrical motor drives the blower through a belt drive which also acts as speed multiplier. The design values of volume flow rate, total pressure, and speed are of 600 m^3/h, 0.5 bar, and 7,500 rpm, respectively.

The blower was designed considering the air incompressible and using the classical design theories [1, 2, 3, 4]. It was aimed at keeping the design as simple as possible in order to simplify the manufacturing process and reduce the manufacturing costs. Each impeller has an entry diameter of 157 mm and an exit diameter of 474 mm. The height of the blade channels decreases from 26 mm at impeller entry to 4 mm at impeller exit. The blade angles are of 32° at entry and 45° at exit. Both impellers have 26 blades, 13 of which are splitter blades. All blades have a thickness of 4 mm. Each scroll case was constructed using four circular arcs. The intake and discharge flanges of each stage have rectangular cross-sections of 140×80 mm^2 and 80×40 mm^2, respectively. The impellers were designed as semi-open, with blades shaped in form of circular arcs. They were machined on a CNC with and end-mill cutter in order to assure the stiffness and proper balancing required by the high operating speed. Special attention was paid at keeping the blade tip clearance as small as possible in order to diminish as much as possible the volume losses. The design solution with back to back mounted impellers leads to constraints regarding the separation of the two stages and the sealing between them, the proper alignment between the impellers mounted on the same shaft and

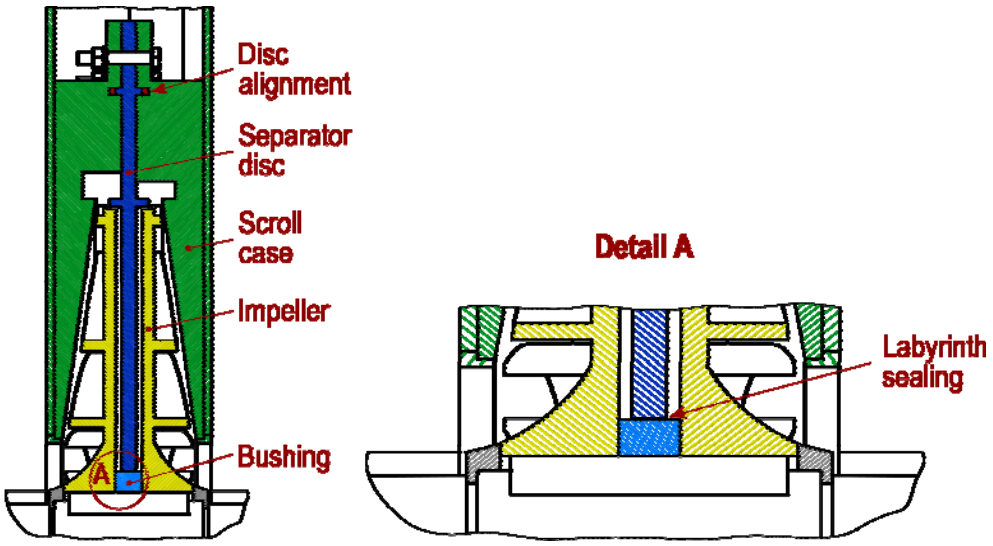

Fig. 2. Blower cross-section.

their scroll casings, and the angular offset between the stages required to allow the proper installation of the connection pipe. The stages are separated by a central disc aligned close to its periphery with the two scroll casings and fastened with them by bolts and nuts (Fig. 2). The disc has a central bore for the shaft. A labyrinth sealing was used to seal the clearance between disc and shaft.

In the following, numerical simulations of the air flow through the blower, carried out for verifying the design, as well as results of subsequent laboratory tests on the blower are presented. The numerical problem is formulated in terms of computational domain and computational grid, governing equations and boundary conditions, air parameters, and numerical models and algorithms used. Numerical results are presented and discussed. The procedure used for laboratory tests is then presented and numerical and experimental results are compared. Conclusions regarding the expected performance of the blower are drawn.

2. Problem formulation

As mentioned in the Introduction, the numerical simulations aim firstly at verifying that the blower can deliver the volume flow rate and pressure considered for design point. Secondly, the simulations could also offer a better insight into the flow inside the impeller blade channels and scroll casing. Of main interest is the structure of the relative vortex that usually forms inside impeller channels, having a detrimental effect on the performance of the turbomachine. There is also of interest to investigate whether a recirculation appears or not between the scroll

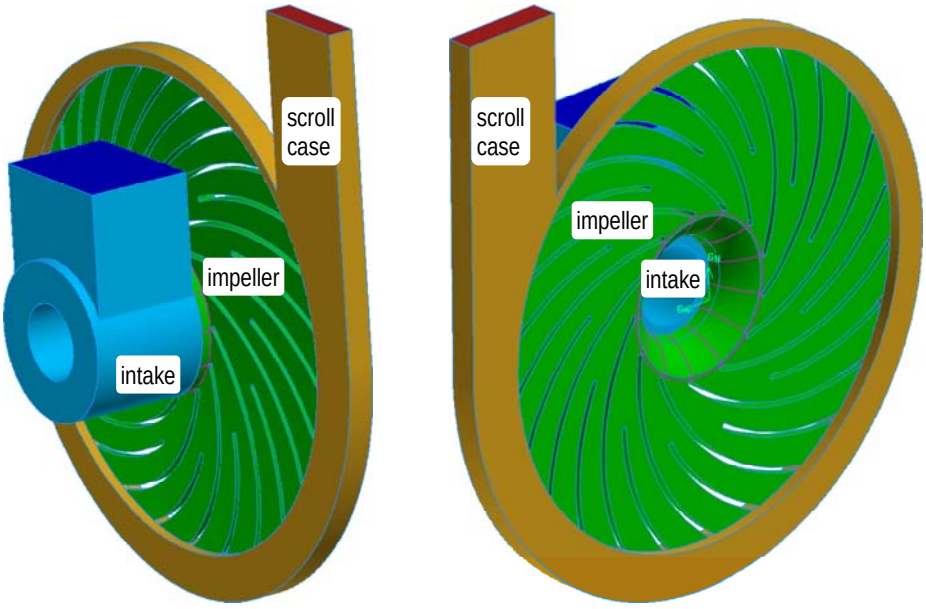

a) b)

Fig. 3. Computational domain for blower intake and first stage: a) front view, b) back view.

case tongue and the discharge section, since such a recirculation has also a negative influence on performance.

The blower has a complicated geometry. Therefore, accurate numerical simulations require a computational grid consisting in a very large number of cells. In the process of creating the grid, special attention must be paid to the regions very close to the solid walls, as well as to the regions where large gradients of the flow parameters are expected, such as at impeller entry and exit and close to the scroll case tongue. In order to reduce the computational time and the computational resources expressed mainly in terms of allocated RAM, only the intake and the first stage of the blower were considered for numerical simulations. Since the two stages of the blower form a serial arrangement, according to the theory and practice of turbomachinery (e.g. [5]) the total volume flow rate of the blower is expected to be practically equal to the volume flow rate of the first stage, while the total pressure increase is expected to be roughly equal to twice the pressure increase of the first stage.

The computational domain chosen to numerically simulate the flow through the intake and the first stage of the blower is depicted in Figure 3. This domain consists in the internal space occupied by the pumped air and is bounded by the internal solid walls of the intake, impeller hub, and scroll case and by the pressure and suction surfaces of the impeller blades.

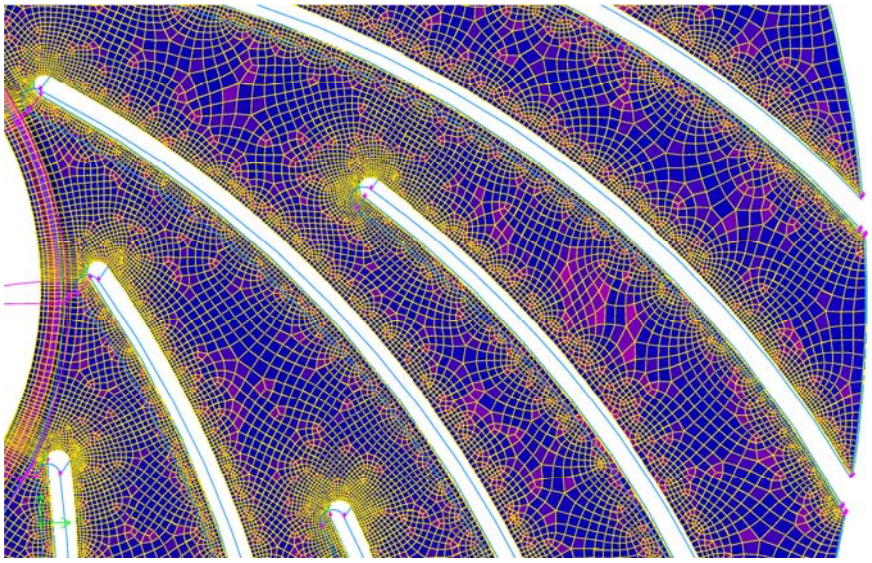

Fig. 4. Detail of computational grid inside impeller.

In order to stay as close to reality as possible, the simulations were performed using the sliding (or dynamic) mesh technique. For this purpose, the intake, the runner and the scroll case form three independent sub-domains that were meshed separately. These sub-domains are separated by special interfaces that allow the transport of the flow parameters, as documented in literature [6]. The meshes of the intake and scroll case are fixed, while the mesh of the runner is allowed to rotate at an angular speed equal to the design angular speed of the blower. Two reference systems are used. The equations of the flow through intake and scroll case are solved in an inertial, fixed reference system, while the equations of the flow through the impeller are solved in a non-inertial reference system that rotates with the impeller.

The computational sub-domains were meshed with unstructured grids using cells of boundary layer type and size functions close to the solid walls and in the regions were sharp gradients are expected, such as at scroll case tongue. For meshing, the program Gambit was used. The resulting grids have a number of roughly 161,000 cells inside the intake, 1,460,000 cells inside the impeller, and 531,000 cells inside the scroll case. A detail of the computational grid inside the impeller is presented in Figure 4.

The air was treated as a compressible gas and the flow was considered turbulent. Due to impeller movement the flow is unsteady. Therefore, the equations governing the three-dimensional, unsteady, compressible, and turbulent flow are the continuity, momentum, and energy equations to which the equation of state must be added as well as the equations describing the chosen turbulence

model. The Reynolds Stress Model (RSM) with standard wall functions and viscous heating was chosen to provide the closure equations for the turbulence quantities. This model adds six equations for the Reynolds (or turbulent) stresses and two equations for the turbulence kinetic energy and its dissipation rate.

As intake boundary condition a total relative pressure p_{ti} of 0 Pa was imposed. Different values of the relative static pressure p_{sd} were set at discharge in order to simulate different operating points. These values are as follows: 5,000 Pa, 10,000 Pa, 15,000 Pa, 20,000 Pa, and 25,000 Pa. Since for 25,000 Pa a reversed flow occurred, additional simulations were performed for p_{sd} values of 24,000 Pa, 23,000 Pa, 22,000 Pa, and 21,000 Pa. On the intake and discharge boundaries, the turbulence kinetic energy and its dissipation rate were calculated based on imposed turbulence intensities and hydraulic diameters. In the absence of any experimental data, it was assumed that the turbulence intensity is of 0.1% at intake and of 2% at discharge. The hydraulic diameters were calculated based on the dimensions of the intake and discharge flanges mentioned previously.

The initial values of all flow variables were set equal to 0.

As operating pressure the value $p_0 = 101{,}325$ Pa was set. The air was considered an ideal gas. Its parameters – specific heat at constant pressure, heat transfer coefficient, and dynamic viscosity – were set as piecewise linear functions using the tabular data presented by Baehr and Stephan [7].

The flow equations in their integral form were integrated in space and time using the finite volume method implemented in the program Ansys Fluent. Since the compressibility effects are far from being critical, a segregated pressure-based solver was chosen using the SIMPLE algorithm for pressure-velocity coupling. The continuity, momentum, and energy equations were discretized in space using a second order upwind scheme, while the RSM equations were discretized with a first order upwind scheme. All equations were discretized in time using a first-order implicit scheme. A time step of 7.5×10^{-5} s was chosen, so that the time stepping frequency is more than four times higher than the blade passing frequency. For each time step it was considered that the solution converged after the scaled residuals of all governing equations dropped below 10^{-3}. The simulations advanced in time until a stabilization of the mass flow rate around an average value was observed for 600 time steps, which is equivalent to roughly 6 impeller revolutions.

Since the design speed of 7,500 rpm is relatively high, the simulations started with a speed as low as 10 rpm and a static discharge pressure of 0 Pa in order to avoid convergence issues. The speed and discharge pressure were increased then progressively, until the first operating point was reached at 7,500 rpm and 5,000 Pa. Afterwards, the discharge pressure was varied as mentioned previously. At each new operating point, the last converged solution of the previous operating point was used as initial guess.

3. Numerical results and discussion

Due to the progressive start-up, no convergence issues were encountered. The average number of iterations required to reach the imposed convergence criteria at each time step was of about 16. A typical convergence history is presented in Figure 5.

When examining the results, typical pressure distributions inside the impeller and scroll case were found. Figure 6 shows pressure contours in a plane that is located 2 mm in front of the impeller back plate. It can be seen that the pressure rises gradually inside the blade channels and, as expected, at any radius the pressure is higher on the pressure side of the blades. Though, the pressure distribution possesses no rotation symmetry, which is the most evident at lower discharge pressures (Fig. 6a). One explanation could be the simple construction of the scroll case, made of four circular arcs, due to which the flow rate profile at impeller exit is not constant. Hence the velocity and pressure profiles are not constant as well.

Of a particular interest is the relative flow inside the blade channels and the relative vortices that form here usually due to flow separation at the pressure sides of the blades under the combined effect of inertial forces (centrifugal and Coriolis), diffuser angle of the blade channel, and pressure increase with radius. The relative vortices have a detrimental effect since the larger they are the more energy they dissipate. In our case, Figure 7 shows that flow separation occurs only before the splitter blades and that the flow reattaches inside the channels formed with the splitter blades. It is interesting to note that the flow separates mainly at

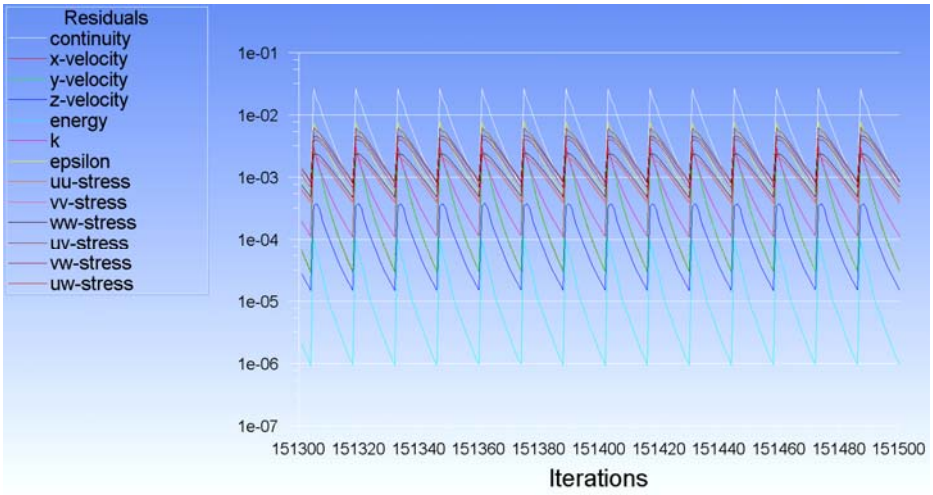

Fig. 5. Convergence history for the last time steps at p_{sd} = 20,000 Pa.

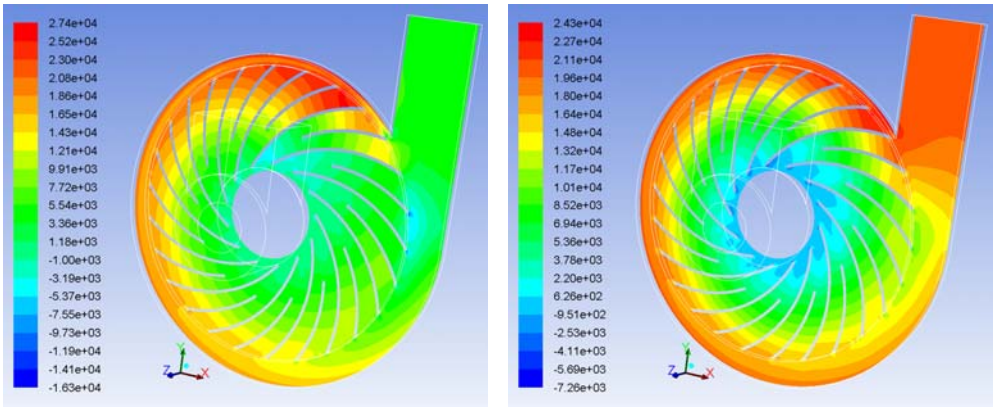

a) b)

Fig. 6. Pressure contours inside impeller and scroll case: a) p_{sd} = 5,000 Pa, b) p_{sd} = 20,000Pa.

the suction sides of the longer blades. As the blades pass by the scroll tongue, the vortices formed due to separation have a smaller extent and the relative flow remains smooth (Fig. 7a). As the blades reach positions diagonally opposed to the scroll case, the separation becomes more complex and the flow more tortuous (Fig. 7b). Nevertheless, we consider that the expected positive effect of the splitter blades is evident.

Global parameters at intake and discharge – mass flow rate, static pressure, and static temperature – as well as the moment exerted by the flowing fluid on the impeller were extracted from the simulations in form of time averaged values. These were used to assess the performance of the analyzed blower stage. The results are summarized in form of performance curves in Figure 8. All calculations required to obtain the curves were made in accordance to EUROVENT norms [8].

Figure 8a presents the pressure curve, i.e. the total pressure increase delivered by the stage depending on mass flow rate. It should be reminded that, when increasing the discharge pressure from 20,000 Pa to 25,000 Pa, a reversed flow occurred. The reversed flow was then encountered even when the discharge pressure was gradually diminished to 21,000 Pa in steps of 1,000 Pa. This is the explanation of the points at negative mass flow rates on the pressure curve. A fourth order polynomial was used to fit the data corresponding both to normal operation and to operation at reversed flow. The fit curve shows that the maximum total pressure expected to be delivered by the stage is only slightly lower than 25,000 Pa, which means that the blower might be able to deliver a total pressure close to the design pressure. In the same time, the corresponding mass flow rate is of about 0.2 kg/s. Under the design conditions of normal atmospheric pressure and 20°C, for which air density roughly equals 1.2 kg/m^3, the value of

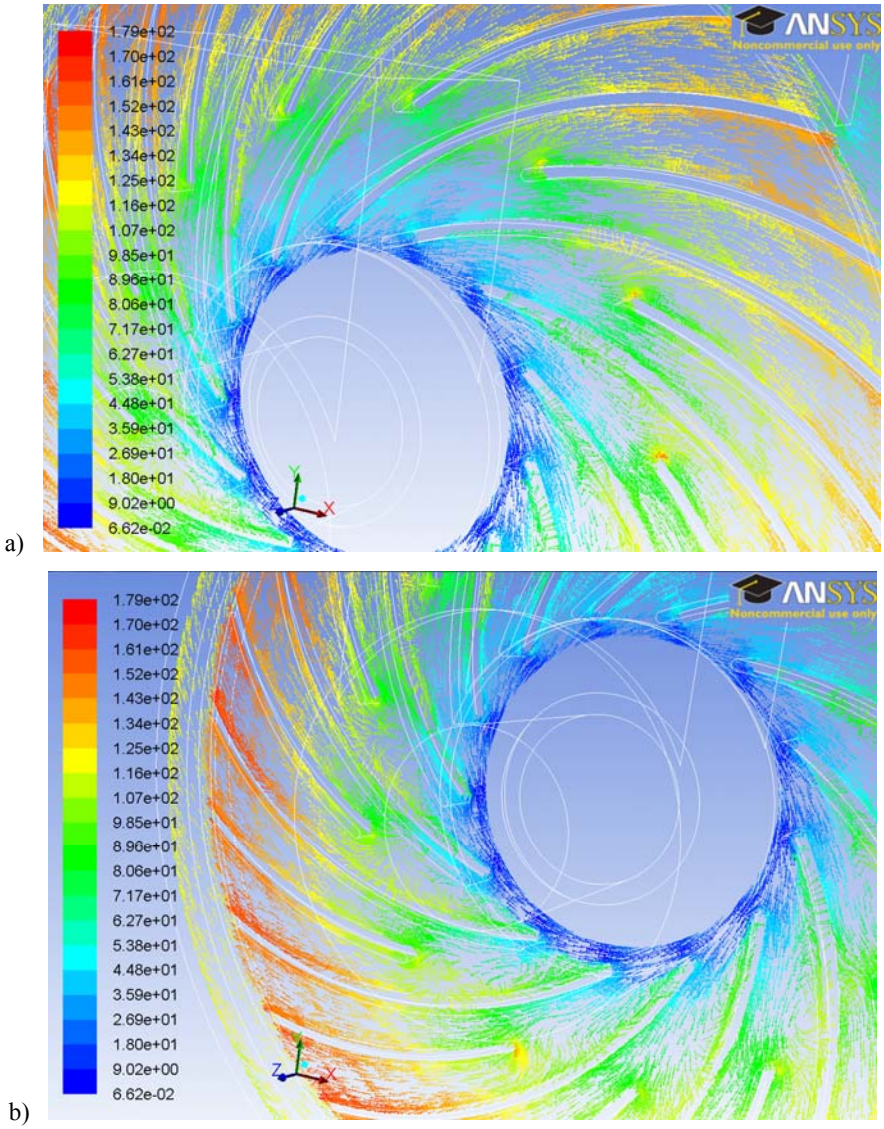

Fig. 7. Vectors of relative velocity inside impeller for p_{sd} = 20,000Pa.

the mass flow rate corresponds to a volume flow rate of about 600 m^3/h. Thus, we can conclude that the blower is expected to reach the performance for which it was designed. It should be noted here that the polynomial fit of the pressure curve suggests that the blower might be prone to surge when improperly operated.

Fig. 8. Performance curves of the blower stage simulated numerically: a) pressure curve; b) power curve; c) efficiency curve

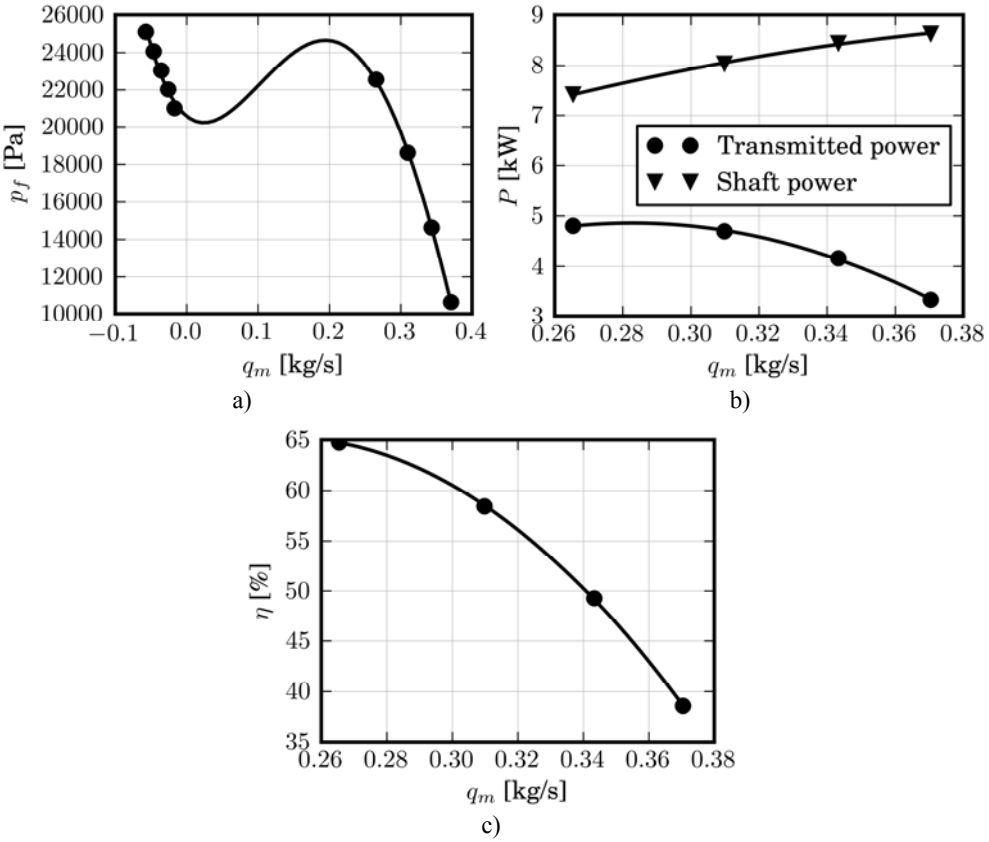

Fig. 8b shows estimated power curves. Transmitted power was calculated using the time averaged global parameters at discharge and intake. It has the ascending trend typical to a centrifugal turbomachine. Shaft power was calculated based on angular speed and time averaged values of the moment exerted by the fluid on the impeller. By dividing shaft power to transmitted power, the expected internal efficiency was calculated. Its curve is presented in Figure 8c. The efficiency shows values that are quite common for centrifugal turbomachines.

4. Performance tests and comparison with numerical results

Since the results of the numerical simulations showed that the blower will most probably be able to deliver the desired pressure and volume flow rate, there was no reason to change the initial design and the next step was to manufacture the machine. The prototype was then subjected to laboratory tests in order to find its real performance. For the tests, the prime mover available to drive the blower was a direct current electrical motor that offered together with the belt drive a maximum

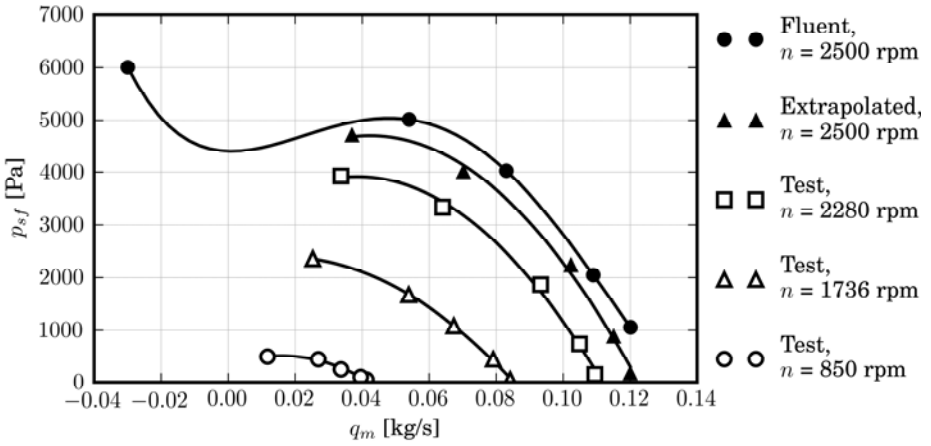

Fig. 9. Comparison between test data and numerical results at operating speeds up to 2500 rpm.

operating speed that was found to be limited to less than 3,000 rpm. Under these conditions, the tests only aimed at verifying the numerical algorithms employed for the numerical simulations.

A new set of simulations was performed keeping unchanged all the algorithms and parameters except the speed and outlet boundary conditions. The speed was changed to 2,500 rpm and simulations were made for discharge pressures of 500 Pa, 1,000 Pa, 2,000 Pa, 2,500 Pa, and 3,000 Pa. In the same time, performance tests were carried out at different blower speeds. All measurements were made according to EUROVENT norms [9]. The volume flow rate was varied by changing the flow area at blower discharge. For each operating point obtained, the increase in static pressure delivered by the blower was measured using a U-tube differential manometer. The volume flow rate was determined by measuring and integrating the velocity profile at blower inlet. To measure the velocity profile a small hot wire anemometer was used.

Fig. 9 shows the measured increase in static pressure depending on volume flow rate at operating speeds of 850 rpm, 1736 rpm, and 2,280 rpm. It was not possible to increase the speed above 2,280 rpm. Therefore, the volume flow rate and the increase in static pressure were extrapolated based on the following formulas [2]:

$$\frac{n'}{n} = \frac{q'_v}{q_v} \qquad \text{and} \qquad \left(\frac{n'}{n}\right)^2 = \frac{p'_{sf}}{p_{sf}}, \tag{1}$$

where , $n' = 2500$ rpm, q_v and p_{sf} are measured volume flow rate and increase in static pressure, respectively, at 2280 rpm and q'_v and p'_{sf} are extrapolated volume flow rate and extrapolated increase in static pressure, respectively, at 2,500 rpm. The extrapolated increase in static pressure is also shown in Figure 9 together with

the increase in static pressure obtained by numerical simulations. Since the numerical simulations were carried out for only one stage of the blower, the curve presented in Fig. 9 was obtained by multiplying with 2 (the number of stages) the increase in static pressure obtained numerically.

As Fig. 9 shows, there is a difference between the extrapolation of the measured pressures and the pressures obtained numerically. On average, this difference is of about 500 Pa and increases towards larger volume flow rates. One important explanation for this difference, besides extrapolation and numerical errors, is given by the fact that, due to simulating only one stage of the blower, the numerical results do not account for the losses inside the duct that links the two stages. Hence, the difference between the increases in static pressure is to be expected. That being said, we can conclude that the numerical results are in good agreement with the results of the laboratory tests.

5. Conclusions

In this paper a new design of a two stage blower for tank aerators was verified by numerical simulations carried out for one stage of the blower operating at the rated speed of 7,500 rpm. The results of the simulations validated the design solution. Consequently, a prototype blower was manufactured and tested. For technical reasons, the prototype could only reach a maximum speed of 2,280 rpm, which is below the rated one. Even so, results of additional numerical simulations, carried out for a speed of 2,500 rpm were found to be in good agreement with extrapolated test results. This validates the numerical algorithms used and allows us to conclude that the prototype blower operating at its rated speed will deliver a pressure and a volume flow rate that will be fairly close to the design values.

R E F E R E N C E S

[1]. *C. Pfleiderer, H. Petermann*, Turbomachinery (in German), 6th Edition, Springer, Berlin, 1991.
[2]. *B. Eck*, Fans: Design and Operation of Centrifugal Axial Flow and Cross Flow Fans (in German), 4th Edition, Springer, Berlin, 1962.
[3]. *V.F. Ris,* Centrifugal Compressors (in Romanian), Editura Tehnică, Bucharest, 1958.
[4]. *R. Neacşu,R., A. Ciocănea,* Computation, design, and testing of pumps, fans, blowers, and compressors, Vol. 1 Radial Turbomachinery (in Romanian), Dacia Press, Cluj-Napoca, 2000.
[5]. *M. Exarhu*, Hydraulic and Pneumatic Machinery and Installations (in Romanian), Agir Press, Bucharest, 2006.
[6]. *** Ansys Fluent Theory Guide, Release 14.0, Ansys Inc., Canonsburg, 2011.
[7]. *H.D. Baehr, K. Stephan*, Heat and Mass Transfer (in German), 3rd Edition, Springer, Berlin, 1998.
[8]. *** EUROVENT 1/4, Terminology of Fan Air Performance Parameters and Operating Characteristics, EUROVENT/CECOMAF, 1994.
[9]. *** EUROVENT 1/6, Guide to the ISO 5801 "Industrial fans – performance testing using standardized airways", EUROVENT/CECOMAF, 1997.